

# Trapped Resonant Fermions above Superfluid Transition Temperature

Chi-Ho Cheng and Sung-Kit Yip

*Institute of Physics, Academia Sinica, Taipei, Taiwan*

(Dated: November 6, 2018)

We investigate trapped resonant fermions with unequal populations within the local density approximation above the superfluid transition temperature. By tuning the attractive interaction between fermions via Feshbach resonance, the system evolves from weakly interacting fermi gas to strongly interacting fermi gas, and finally becomes bose-fermi mixture. The density profiles of fermions are examined and compared with experiments. We also point out the simple relationships between the local density, the axial density, and the gas pressure within the local density approximation.

PACS numbers: 03.75.Ss, 05.30.Fk, 34.90.+q

The experimental investigation of the crossover from the Bardeen-Cooper-Schrieffer (BCS) state to the Bose-Einstein Condensation (BEC) state induced by Feshbach resonance for trapped fermionic atomic gases with equal [1, 2, 3, 4, 5] and unequal populations [6, 7, 8] have attracted lots of interests from the physics community. For equal populations, the ground state of the system evolves from weak-coupling BCS to strong-coupling BEC as the effective attraction between two species of fermions becomes strong [9, 10, 11, 12, 13, 14]. In the case of unequal populations of the two fermion species, the system evolves from a normal state, through a spatially inhomogeneous state(s) (like Fulde-Ferrell-Larkin-Ovchinnikov (FFLO) state and/or phase separation) in the weak-coupling regime to a bose-fermi mixture in the strong-coupling regime [15, 16, 17, 18, 19, 20, 21, 22, 23].

Although mean-field treatments can provide a qualitative picture, inclusion of fluctuations [9] around the mean-field solution is necessary to give results with more quantitative agreement with experiments. For example, thermodynamics [24, 25] and density profiles [13, 14] at finite temperature can be properly accounted for only when pair fluctuations are included. Including these fluctuations [26, 27] can also give a reasonable value for the zero-temperature universal [28, 29] parameter  $\beta$  at resonance, though it does not match exactly with the Quantum Monte-Carlo results [12, 30, 31].

Till now, most of the studies are below the superfluid transition temperature. However, above the transition temperature, the normal fermion gas can still be strongly interacting and becomes a mixture of bose and fermi gases in the strong coupling regime. The system provides a good testing ground for strongly interacting many-body theories.

On the other hand, the thermometry of strongly interacting fermi gas is also important and difficult in experiments [24]. In the case of non-interacting fermions, the temperature can be simply measured by fitting the density profile of trapped fermions with the Thomas-Fermi distribution. Thermometry of strongly interacting fermions with equal populations requires non-trivial

fitting procedure on the theoretically generated density profiles [25]. In the case of unequal populations of two species of fermions, the wing of the majority component (excess fermion) becomes non-interacting due to the absence of the minority component, and thus can be served as a good thermometer [8].

In this paper, the Nozieres-Schmitt-Rink (NSR) formalism [9] is adopted since it is the simplest theory that can continuously bring both the BCS and BEC regimes respectively for weak and strong coupling limits together at finite temperatures, and also gives a good estimate of the universal parameter in the unitarity limit as stated above. The harmonic trapping potential is considered within the local density approximation (LDA).

We found that the Hartree-Fock approximation is recovered in the weak-coupling regime, but it is qualitatively different from the NSR treatment if the system evolves into a strongly interacting fermi gas. In the strong coupling limit, the system becomes a bose-fermi mixture. An effective repulsion between the bosonic molecules and fermions emerges from the NSR theory. Not so surprisingly, a similar repulsive effect also exists in the intermediate coupling regime from the NSR theory although no bound pair is formed. The density profiles are obtained, comparison and implication to the recent experiment are then discussed.

We adopted the implementation of the NSR formalism by the functional integral method [10]. The action of our system is written as

$$S = \int d\tau d\vec{r} \left\{ \sum_{\sigma} \bar{\psi}_{\sigma} (\partial_{\tau} - \nabla^2/2m - \mu_{\sigma} + V(\vec{r})) \psi_{\sigma} + g \bar{\psi}_{\uparrow} \bar{\psi}_{\downarrow} \psi_{\downarrow} \psi_{\uparrow} \right\} \quad (1)$$

with attractive coupling constant  $g < 0$ .  $\sigma$  runs over up and down spin species, and  $\psi_{\sigma} \equiv \psi_{\sigma}(\vec{r}, \tau)$  are the fermionic fields. Two chemical potentials  $\mu_{\sigma}$  fix the fermion number densities inside the trapping potential  $V(\vec{r})$ .

By introducing the Hubbard-Stratonovich field  $\Delta(\vec{r}, \tau)$  coupled to the pairing field  $\bar{\psi}_{\uparrow} \bar{\psi}_{\downarrow}$ , and then integrating

out the fermion fields  $\psi_\sigma$ , we get the effective action in terms of  $\Delta(\vec{r}, \tau)$ . Above the superfluid transition temperature with vanishing saddle point  $\Delta_0 = 0$ , we expand the effective action around the saddle point up to the Gaussian level in  $\Delta(\vec{q}, \hat{p}_n)$ , which gives

$$S_{\text{eff}} = S_0 + \sum_{\vec{q}, \hat{p}_n} \Gamma^{-1}(\vec{q}, \hat{p}_n) |\Delta(\vec{q}, \hat{p}_n)|^2 \quad (2)$$

where

$$\Gamma^{-1}(\vec{q}, \hat{p}_n) = \frac{1}{L^3} \sum_{\vec{k}} \left( \frac{1 - n_{\text{F}}(\xi_{\vec{q}/2+\vec{k}, \uparrow}) - n_{\text{F}}(\xi_{\vec{q}/2-\vec{k}, \downarrow})}{\hat{p}_n - \xi_{\vec{q}/2+\vec{k}, \uparrow} - \xi_{\vec{q}/2-\vec{k}, \downarrow}} + \frac{1}{2\epsilon_{\vec{k}}} \right) - \frac{m}{4\pi a} \quad (3)$$

with  $\epsilon_{\vec{k}} = k^2/2m$ ,  $\xi_{\vec{k}, \sigma} \equiv \epsilon_{\vec{k}} - \mu_\sigma + V(\vec{r})$ , and  $n_{\text{F}}$  is the Fermi distribution function. The  $s$ -wave scattering length  $a$  defined by two-body low-energy scattering via  $m/4\pi a = 1/g + L^{-3} \sum_{\vec{k}} 1/2\epsilon_{\vec{k}}$  is to regulate the ultraviolet divergence. Following Nozières and Schmitt-Rink [9], we can rewrite the free energy

$$F = F_0 - \frac{1}{L^3} \sum_{\vec{q}} \int_{-\infty}^{+\infty} \frac{d\omega}{\pi} n_{\text{B}}(\omega) \delta(\vec{q}, \omega) \quad (4)$$

in terms of the phase shift  $\delta(\vec{q}, \omega)$  defined by  $\Gamma(\vec{q}, \omega + i0^+) = |\Gamma(\vec{q}, \omega)| \exp(i\delta(\vec{q}, \omega))$ .  $F_0$  is the free energy of free fermions and  $n_{\text{B}}$  is the Bose distribution function. The number equations are given by

$$n_\sigma(\vec{r}) = n_\sigma^0(\vec{r}) + \frac{1}{L^3} \sum_{\vec{q}} \int_{-\infty}^{+\infty} \frac{d\omega}{\pi} n_{\text{B}}(\omega) \frac{\partial}{\partial \mu_\sigma} \delta(\vec{q}, \omega) \quad (5)$$

with the bare occupation  $n_\sigma^0(\vec{r}) = L^{-3} \sum_{\vec{k}} n_{\text{F}}(\xi_{\vec{k}, \sigma})$ .

Our density profiles are calculated from Eq.(5). To clarify the physics, we first examine two limiting cases. In the extreme weak coupling limit with  $a < 0$  and  $k_{\text{F}}|a| \ll 1$ ,  $\Re\Gamma^{-1} \simeq -m/4\pi a$ , with the first term in Eq.(3) contributing a small imaginary part. Hence

$$\delta(\vec{q}, \omega) \simeq \frac{4\pi a}{m} \Im m \Gamma^{-1}(\vec{q}, \omega) \quad (6)$$

and the second term in Eq.(5) becomes

$$\begin{aligned} & \frac{4\pi a}{m} \frac{\partial}{\partial \mu_\sigma} \frac{1}{L^3} \sum_{\vec{q}} \int_{-\infty}^{+\infty} \frac{d\omega}{\pi} n_{\text{B}}(\omega) \Im m \Gamma^{-1}(\vec{q}, \omega) \\ &= -\frac{4\pi a}{m} \frac{\partial}{\partial \mu_\sigma} \frac{1}{L^6} \sum_{\vec{q}, \vec{k}} n_{\text{B}}(\xi_{\vec{q}/2+\vec{k}, \uparrow} + \xi_{\vec{q}/2-\vec{k}, \downarrow}) \\ & \quad \times (1 - n_{\text{F}}(\xi_{\vec{q}/2+\vec{k}, \uparrow}) - n_{\text{F}}(\xi_{\vec{q}/2-\vec{k}, \downarrow})) \\ &= -\frac{4\pi a}{m} \frac{\partial}{\partial \mu_\sigma} \frac{1}{L^6} \sum_{\vec{q}, \vec{k}} n_{\text{F}}(\xi_{\vec{q}/2+\vec{k}, \uparrow}) n_{\text{F}}(\xi_{\vec{q}/2-\vec{k}, \downarrow}) \\ &= -\frac{4\pi a}{m} n_{-\sigma}^0(\vec{r}) \frac{\partial}{\partial \mu_\sigma} n_\sigma^0(\vec{r}) \quad (7) \end{aligned}$$

where the bose distribution function is eliminated by the identity,  $n_{\text{B}}(x+y)(1-n_{\text{F}}(x)-n_{\text{F}}(y)) = n_{\text{F}}(x)n_{\text{F}}(y)$ . The occupation in Eq.(5) reduces to

$$\begin{aligned} n_\sigma(\vec{r}) &\simeq n_\sigma^0(\vec{r}) - \frac{4\pi a}{m} n_{-\sigma}^0(\vec{r}) \frac{\partial}{\partial \mu_\sigma} n_\sigma^0(\vec{r}) \\ &\simeq \frac{1}{L^3} \sum_{\vec{k}} n_{\text{F}}(\xi_{\vec{k}, \sigma} + \frac{4\pi a}{m} n_{-\sigma}^0(\vec{r})) \quad (8) \end{aligned}$$

The expression is equivalent to the first-order Hartree-Fock (HF) approximation to the original Hamiltonian in Eq.(1) with the effective coupling constant  $4\pi a/m$  instead of the bare  $g$ .

In Fig. 1, we plot both the density profiles of the NSR and HF theories. At extremely small  $k_{\text{F}}|a|$ , as shown in Fig. 1(c), two theories coincide with each other. As the interaction parameter increases,  $\Re\Gamma^{-1} > -m/4\pi a$  due to the contribution from the first term in Eq.(3). The HF approximation overestimates the effective attractive interaction. As shown in Fig. 1(b), the HF results for the minority component lies above our fluctuation theory results near the trap center. The deviations between these two theories are larger for the minority than the majority component, since the minority component actually feels a larger change in effective particle energy (see the argument of the function  $n_{\text{F}}$  in Eq.(8)).

Upon further increase in  $k_{\text{F}}|a|$  (Fig. 1(a)), the NSR theory shows even qualitative disagreement with the HF results. It can be seen that the majority profile from NSR theory lies *above* the HF results near the trap center. The reason of the disagreement will be discussed further below.

In the strong coupling limit where  $a > 0$ , the two-particle vertex function  $\Gamma(\vec{q}, \omega)$  acquires a discrete pole  $\omega = \omega_{\text{b}}(\vec{q})$  representing the bound state of fermion-pair. Around the pole, we can write

$$\Gamma(\vec{q}, \omega) = \frac{R}{-\omega + \omega_{\text{b}}(\vec{q})} \quad (9)$$

with small  $\vec{q}$ , and the dispersion  $\omega_{\text{b}}(\vec{q}) = c_0 + c_1 q^2$ . Eq.(9) can also be written as

$$\omega_{\text{b}}(\vec{q}) - \omega = R \Gamma^{-1}(\vec{q}, \omega) \quad (10)$$

The coefficient  $c_0$  can be determined from putting  $\vec{q} = 0$ ,  $\omega = c_0$  into Eq.(10), which gives  $\Gamma^{-1}(0, c_0) = 0$ , *i.e.*,

$$\frac{1}{L^3} \sum_{\vec{k}} \left( \frac{1 - n_{\text{F}}(\xi_{\vec{k}, \uparrow}) - n_{\text{F}}(\xi_{\vec{k}, \downarrow})}{c_0 - \xi_{\vec{k}, \uparrow} - \xi_{\vec{k}, \downarrow}} + \frac{1}{2\epsilon_{\vec{k}}} \right) = \frac{m}{4\pi a} \quad (11)$$

We rewrite this formula as

$$\frac{1}{L^3} \sum_{\vec{k}} \left( \frac{1}{(c_0 + \mu_{\uparrow} + \mu_{\downarrow} - 2V(\vec{r})) - 2\epsilon_{\vec{k}}} + \frac{1}{2\epsilon_{\vec{k}}} \right) - \frac{1}{L^3} \sum_{\vec{k}} \frac{n_{\text{F}}(\xi_{\vec{k},\uparrow}) + n_{\text{F}}(\xi_{\vec{k},\downarrow})}{(c_0 + \mu_{\uparrow} + \mu_{\downarrow} - 2V(\vec{r})) - 2\epsilon_{\vec{k}}} = \frac{m}{4\pi a} \quad (12)$$

With equal population, the chemical potential of the bound state  $\mu_{\uparrow} = \mu_{\downarrow} < 0$ , the second term of the L.H.S. of Eq.(12) vanishes at temperature  $k_{\text{B}}T \ll |\mu_{\uparrow,\downarrow}|$ . There we can obtain  $c_0 = \epsilon_{\text{b}} - \mu_{\uparrow} - \mu_{\downarrow} + 2V(\vec{r})$ , with the binding energy  $\epsilon_{\text{b}} = -1/ma^2 < 0$ . In our case of unequal populations, the chemical potential of excess (unpaired) fermions  $\mu_{\uparrow} > 0$  and that of the bound state  $\mu_{\downarrow} < 0$ . For temperatures  $k_{\text{B}}T \ll |\epsilon_{\text{b}}|$ , we can substitute the above  $c_0$  of equal population into the second term of the L.H.S. of Eq.(12), ignore  $\epsilon_{\vec{k}}$  in the denominator, and obtain for this term  $-ma^2\delta n_{\text{f}}^0(\vec{r})$ , where  $\delta n_{\text{f}}^0(\vec{r}) \equiv L^{-3} \sum_{\vec{k}} n_{\text{F}}(\xi_{\vec{k},\uparrow})$  can be interpreted as the occupation due to bare excess fermion. Eq.(12) then gives

$$\begin{aligned} & \frac{1}{L^3} \sum_{\vec{k}} \left( \frac{1}{(c_0 + \mu_{\uparrow} + \mu_{\downarrow} - 2V(\vec{r})) - 2\epsilon_{\vec{k}}} + \frac{1}{2\epsilon_{\vec{k}}} \right) \\ &= \frac{m}{4\pi a} - ma^2\delta n_{\text{f}}^0(\vec{r}) \end{aligned} \quad (13)$$

hence we get

$$\begin{aligned} c_0 &= -\frac{1}{ma^2}(1 - 4\pi a^3\delta n_{\text{f}}^0(\vec{r}))^2 - \mu_{\uparrow} - \mu_{\downarrow} + 2V(\vec{r}) \\ &\simeq \epsilon_{\text{b}} + g_{\text{bf}}\delta n_{\text{f}}^0(\vec{r}) - \mu_{\uparrow} - \mu_{\downarrow} + 2V(\vec{r}) \end{aligned} \quad (14)$$

with  $g_{\text{bf}} \equiv 8\pi a/m$ .

Similarly,  $R$  can be determined by putting  $\vec{q} = 0$  and taking the limit  $\omega \rightarrow c_0$  in Eq.(10),

$$\begin{aligned} R^{-1} &= \lim_{\omega \rightarrow c_0} \frac{\Gamma^{-1}(0, \omega)}{c_0 - \omega} \\ &= \frac{1}{L^3} \sum_{\vec{k}} \frac{1 - n_{\text{F}}(\xi_{\vec{k},\uparrow}) - n_{\text{F}}(\xi_{\vec{k},\downarrow})}{(\epsilon_{\text{b}} + g_{\text{bf}}\delta n_{\text{f}}^0(\vec{r}) - 2\epsilon_{\vec{k}})^2} \\ &\simeq \frac{m^2 a}{8\pi} (1 - 4\pi a^3\delta n_{\text{f}}^0(\vec{r})) \end{aligned} \quad (15)$$

By noticing that, in the denominator of the first term in Eq.(3), the  $q^2$ -term can be combined with  $\dot{\psi}_n$ , we found  $\Gamma^{-1}(\vec{q}, \omega) = \Gamma^{-1}(0, \omega - q^2/4m) + O(q^4)$ . Therefore  $c_1 = 1/4m$ .

In the strong coupling regime, the low-energy effective action can then be written as

$$S_{\text{eff}} = S_0 + \sum_{\vec{q}, \dot{\psi}_n} (-\dot{\psi}_n + \omega_{\text{b}}(\vec{q})) \bar{\phi}(\vec{q}, \dot{\psi}_n) \phi(\vec{q}, \dot{\psi}_n) \quad (16)$$

where we identify the boson field  $\phi(\vec{q}, \dot{\psi}_n) \equiv R^{-1/2} \Delta(\vec{q}, \dot{\psi}_n)$ , and  $\omega_{\text{b}}(\vec{q}) \equiv \epsilon_{\text{b}} + g_{\text{bf}}\delta n_{\text{f}}^0(\vec{r}) - \mu_{\uparrow} - \mu_{\downarrow} + 2V(\vec{r}) + q^2/4m$ . The phase shift across the pole  $\omega = \omega_{\text{b}}(\vec{q})$

jumps from 0 to  $\pi$ , *i.e.*,  $\delta(\vec{q}, \omega) = \pi\theta(\omega_{\text{b}}(\vec{q}) - \omega)$ . Noticing that

$$\begin{aligned} \frac{\partial}{\partial \mu_{\uparrow}} \delta(\vec{q}, \omega) &= \pi \delta(\omega - \omega_{\text{b}}(\vec{q})) \left( 1 - g_{\text{bf}} \frac{\partial}{\partial \mu_{\uparrow}} \delta n_{\text{f}}^0(\vec{r}) \right) \\ \frac{\partial}{\partial \mu_{\downarrow}} \delta(\vec{q}, \omega) &= \pi \delta(\omega - \omega_{\text{b}}(\vec{q})) , \end{aligned} \quad (17)$$

and then the number equation in Eq.(5) gives

$$\begin{aligned} n_{\uparrow}(\vec{r}) &= \delta n_{\text{f}}^0(\vec{r}) + \left( n_{\text{b}}(\vec{r}) - g_{\text{bf}} n_{\text{b}} \frac{\partial}{\partial \mu_{\uparrow}} \delta n_{\text{f}}^0(\vec{r}) \right) \\ &\simeq \delta n_{\text{f}}(\vec{r}) + n_{\text{b}}(\vec{r}) \end{aligned} \quad (18)$$

and

$$n_{\downarrow}(\vec{r}) = n_{\text{b}}(\vec{r}) \quad (20)$$

with  $\delta n_{\text{f}}(\vec{r}) = L^{-3} \sum_{\vec{k}} n_{\text{F}}(\xi_{\vec{k},\uparrow} + g_{\text{bf}} n_{\text{b}}(\vec{r}))$  and  $n_{\text{b}}(\vec{r}) = L^{-3} \sum_{\vec{q}} n_{\text{B}}(\omega_{\text{b}}(\vec{q}))$ . Eqs.(19)-(20) are the number equations in strong coupling limit. The effective interaction characterized by  $g_{\text{bf}}$  between the bound pairs and residue fermions are already captured in the Gaussian level. The same results were also obtained by a low density zero-temperature expansion by one of the authors [32] and self-consistent Bogoliubov-de-Gennes equations by Pieri and Strinati [19], but this interaction was missing in the treatment of Liu and Hu [20]. Note also that, in NSR formalism,  $n_{\text{b}}(\vec{r})$  and  $\delta n_{\text{f}}(\vec{r})$  are not determined self-consistently. Instead,  $n_{\text{b}}(\vec{r})$  relies (via  $\omega_{\text{b}}(\vec{q})$ ) only on the bare  $\delta n_{\text{f}}^0(\vec{r})$ , and  $\delta n_{\text{f}}(\vec{r})$  depends then on  $n_{\text{b}}(\vec{r})$ .

With the LDA, the density profile of an anisotropic harmonic trap can be mapped to a corresponding isotropic one by rescaling the radial distances for the different axes. In the following, we consider only the isotropic case.

The density profiles of fermions of up and down-spin for different interaction parameter  $-1/k_{\text{F}}a$  are shown in Fig. 2. The total populations of the majority species is  $1.5 \times 10^7$  with the population imbalances 50%,  $T/T_{\text{F}} = 0.2$  in the weak-coupling regimes of Fig. 2(b)-(e). These parameters are chosen to be close to those in an experiment of MIT [8]. As the interaction parameter becomes stronger, the two species of fermions are strongly interacting with each other and the local density at the trap center rises. The excess fermions defined by the difference between the local densities of up and down-spin fermions are repelled from the trap center. Thomas-Fermi fit to the wing of the majority profile are insensitive to the interaction parameter although the fermions density profile

can be strongly deformed. It is an evidence to the reliability of the thermometry from the excess fermions. Because of the attractive interaction from down-spin fermion, the profile of the Thomas-Fermi fit always lies below that of up-spin fermion. When we increase  $k_{\text{F}}a$  further close to the unitarity limit (Fig. 2(b)), there is a dramatic change in density profiles. The bound pairs are close to being bose-condensed. It explains why both species strongly peak near the trap center and the density profiles behave qualitatively differently from that of the HF results, as discussed above. The case of strong coupling regime is shown in Fig. 2(a) where a large population imbalance was chosen to avoid the bose-condensation of the bound pairs.

Near the resonance, the NSR theory may break down due to the unphysical (non-positive definite) susceptibility matrix  $\partial n_{\sigma}/\partial \mu_{\sigma'}$  [23]. We checked that the susceptibility matrix is positive definite with the same parameters used in Fig. 2. The NSR theory does not break down at this point in our problem.

To compare our result more directly with experiments (see Fig. 1 in Ref. [8]), the column densities are shown in Fig. 3. The column density  $n_{\text{col}}(\rho)$  can be obtained from the local density  $n(r)$  by

$$n_{\text{col}}(\rho) \equiv \int_{-\infty}^{\infty} dx n(r) = \int_{\rho}^{\infty} dr \frac{2r}{\sqrt{r^2 - \rho^2}} n(r) \quad (21)$$

We also plot the Thomas-Fermi fit to the wing of the up-spin fermions, and the non-interacting fermions profile with the the same total population and temperature as that of the down-spin fermions. Because of strong attraction around the trap center, the interacting profiles always lie above the non-interacting one near the center.

Compared with a recent experiment [8], we found only some qualitative similarities but also rather significant disagreements. The cloud sizes are found to be smaller than their non-interacting counterparts, as in the experiments. However, experimentally the density profiles deviate from the non-interacting ones mainly for the majority cloud but not so much for the minority cloud, whereas we found significant effects of the attractive interaction on both. Experimentally, the density profile of the majority particles actually lies *below* the finite temperature non-interacting fit of the wings at where the minority component appears, though this deficit decreases when  $1/k_{\text{F}}a$  increases. Our calculated results give a density profile *above* this fit, as expected from attractive interaction between the particles. With increasing  $1/k_{\text{F}}a$ , there is a larger and larger enhancement of the actual density profile over the fit to the wings. A possible source of disagreement is that our current understanding of the expansion dynamics is not sufficiently quantitative, so that the scaling factors for the interacting gas near the center versus that of the non-interacting particles near the wing are different from what was used in Ref. [8].

For the minority component, our density profile shows strong effects of the effective attractive interaction, so that it peaks much more strongly near the trap center than a corresponding non-interacting distribution as seen in Fig. 3. (whereas experimentally it can be fitted well by the non-interacting profile). We found that, even above the transition temperature as it is here, the difference between the majority and minority components (*i.e.*, the excess fermion density) seems to decrease when  $1/k_{\text{F}}a$  increases. This trend already exists in the HF results (see Fig. 1 and discussions above). It can also be understood as an effective repulsive interaction between the bosons on the excess fermions, so that the latter are pushed out from the trap center (*c.f.* Fig. 2, especially 2(a) and (b)), though this effect is not so evident in the column density profile due to the integration.

In the following, we want to point out that, for a harmonic trap within the local density approximation, the axial density (from integration of the local density) directly provides us the local gas pressure  $P$ , and the original local density can be easily read out from the slope of axial density profile. Thus the axial density directly gives us the equation of state ( $P$  as a function of  $n$ ) at the given temperature.

At a given temperature, general thermodynamic relation gives  $dP(r) = n(r)d\mu(r)$  where  $\mu(r) \equiv (\mu_{\uparrow}(r) + \mu_{\downarrow}(r))/2$  (Note that  $\mu_{\uparrow}(r) - \mu_{\downarrow}(r)$  is independent of  $r$ ). Within the LDA, we can view the position  $r$  as a parameter and thus write  $dP(r) = n(r)d\mu(r)$ . Since the effective chemical potential is  $\mu(r) = \mu_0 - V(r)$ , we obtain

$$dP(r) = -n(r)dV(r) \quad (22)$$

This relation can also be obtained by balancing the forces due to the pressure and trap potential acting on a shell of atoms between  $r$  and  $r + dr$ . For a harmonic trap,  $V(r) = (\alpha/2)r^2$ , we therefore get  $dP(r) = -n(r)\alpha r dr$  and by integration

$$P(r) = \alpha \int_r^{\infty} dr' r' n(r') \quad (23)$$

On the other hand, the axial density at  $z$  is defined by

$$n_{\text{axi}}(z) = \int_0^{\infty} 2\pi \rho d\rho n(r) \quad (24)$$

where  $\rho^2 = x^2 + y^2 = r^2 - z^2$ . This can be re-written as

$$n_{\text{axi}}(z) = 2\pi \int_z^{\infty} dr r n(r) \quad (25)$$

Comparing Eqs.(23)-(25) gives

$$P(z) = \frac{\alpha}{2\pi} n_{\text{axi}}(z) \quad (26)$$

The axial density is thus a direct measure of the gas pressure. Also, by taking the derivative of Eq.(25) with

respect to  $z$ , we get

$$\frac{d}{dz}n_{\text{axi}}(z) = -2\pi zn(z). \quad (27)$$

Hence (see also Ref. [18])

$$n(z) = -\frac{1}{2\pi z} \frac{d}{dz}n_{\text{axi}}(z) \quad (28)$$

The axial density thus also gives us the original local density profile [33].

Thus the axial density alone gives us the relation between the gas pressure and density at a given temperature. For completeness, we show also the corresponding axial density profiles in Fig. 4.

[For an axially symmetric trap with potential  $V(\vec{r}) = \frac{1}{2}(\alpha_z z^2 + \alpha\rho^2)$ , the corresponding relations are:  $P(z) = \frac{\alpha}{2\pi}n_{\text{axi}}(z)$  and  $n(0, 0, z) = -\frac{\alpha}{2\pi\alpha_z} \frac{1}{z} \frac{dn_{\text{axi}}(z)}{dz}$ .]

To conclude, we have studied a two-component interacting Fermi gas with interaction induced by a Feshbach resonance above the transition temperature. The density profiles show strong modifications due to the effect of this interaction.

We acknowledge the support from the Academia Sinica and the National Science Council of Taiwan under Grant Nos. NSC94-2112-M-001-002 and NSC95-2112-M-001-054.

- 
- [1] M. Greiner, C.A. Regal, and D.S. Jin, *Nature*, **426**, 537 (2003)
  - [2] M.W. Zwierlein, C.A. Stan, C.H. Schunck, S.M.F. Raupach, S. Gupta, Z. Hadzibabic, and W. Ketterle, *Phys. Rev. Lett.* **91**, 250401 (2003).
  - [3] M. Bartenstein, A. Altmeyer, S. Riedl, S. Jochim, C. Chin, J. Hecker Denschlag, and R. Grimm, *Phys. Rev. Lett.* **92**, 120401 (2004).
  - [4] T. Bourdel, L. Khaykovich, J. Cubizolles, J. Zhang, F. Chevy, M. Teichmann, L. Tarruell, S.J.J.M.F. Kokkelmans, and C. Salomon, *Phys. Rev. Lett.* **93**, 050401 (2004).
  - [5] G.B. Partridge, K.E. Strecker, R.I. Kamar, M.W. Jack, and R.G. Hulet, *Phys. Rev. Lett.* **95**, 020404 (2005).
  - [6] M.W. Zwierlein, A. Schirotzek, C.H. Schunck, and W. Ketterle, *Science* **311**, 492 (2006).
  - [7] G.B. Partridge, W. Li, R.I. Kamar, Y. Liao, and R.G. Hulet, *Science* **311**, 503 (2006).
  - [8] M.W. Zwierlein, C.H. Schunck, A. Schirotzek, and W. Ketterle, *Nature* **442**, 54 (2006).
  - [9] P. Nozières and S. Schmitt-Rink, *J. Low Temp. Phys.* **59**, 195 (1985).

- [10] C.A.R. Sá de Melo, M. Randeria, and J.R. Engelbrecht, *Phys. Rev. Lett.* **71**, 3202 (1993).
  - [11] Y. Ohashi and A. Griffin, *Phys. Rev. A* **67**, 063612 (2003).
  - [12] J. Carlson, S.-Y. Chang, V.R. Pandharipande, and K.E. Schmidt, *Phys. Rev. Lett.* **91**, 050401 (2003).
  - [13] A. Perali, P. Pieri, L. Pisani, and G.C. Strinati, *Phys. Rev. Lett.* **92**, 220404 (2004).
  - [14] J. Stajic, Q. Chen, and K. Levin, *Phys. Rev. Lett.* **94**, 060401 (2005).
  - [15] T. Mizushima, K. Machida, and M. Ichioka, *Phys. Rev. Lett.* **94**, 060404 (2005).
  - [16] C.H. Pao, S.T. Wu, and S.K. Yip, *Phys. Rev. B* **73**, 132506 (2006).
  - [17] D. E. Sheehy and L. Radzihovsky, *Phys. Rev. Lett.* **96**, 060401 (2006)
  - [18] C.H. Pao and S.K. Yip, *J. Phys.: Condens. Matter* **18**, 5567 (2006).
  - [19] P. Pieri and G.C. Strinati, *Phys. Rev. Lett.* **96**, 150404 (2006).
  - [20] X.J. Liu and H. Hu, *Europhys. Lett.* **75**, 364 (2006).
  - [21] T.N. De Silva and E.J. Mueller, *Phys. Rev. A* **73**, 051602(R) (2006).
  - [22] T.N. De Silva and E.J. Mueller, *Phys. Rev. Lett.* **97**, 070402 (2006).
  - [23] M.M. Parish, F.M. Marchetti, A. Lamacraft, and B.D. Simons, *cond-mat/0605744*.
  - [24] J. Kinast, A. Turlapov, J.E. Thomas, Q. Chen, J. Stajic, and K. Levin, *Science* **307**, 1296 (2005).
  - [25] Q.J. Chen, J. Stajic, and K. Levin, *Phys. Rev. Lett.* **95**, 260405 (2005).
  - [26] A. Perali, P. Pieri, and G.C. Strinati, *Phys. Rev. Lett.* **93**, 100404 (2004).
  - [27] R. Haussmann, W. Rantner, S. Cerrito, and W. Zwerger, *cond-mat/0608282*.
  - [28] G.A. Baker, Jr., *Phys. Rev. C* **60**, 054311 (1999).
  - [29] H. Heiselberg, *Phys. Rev. A* **63**, 043606 (2001).
  - [30] S.-Y. Chang, V.R. Pandharipande, J. Carlson, and K.E. Schmidt, *Phys. Rev. A* **70**, 043602 (2004).
  - [31] G.E. Astrakharchik, J. Boronat, J. Casulleras, and S. Giorgini, *Phys. Rev. Lett.* **93**, 200404 (2004).
  - [32] S.K. Yip, *cond-mat/0203582*.
  - [33] The relationship between these two densities in Eq.(28) can also be shown via the Abel transform and its inverse [34] within the LDA. The axial density  $n_{\text{axi}}(z)$  can also be written as
- $$n_{\text{axi}}(z) \equiv \int_{-\infty}^{\infty} dy n_{\text{col}}(\rho = \sqrt{y^2 + z^2}) = \int_z^{\infty} d\rho \frac{2\rho}{\sqrt{\rho^2 - z^2}} n_c(\rho)$$
- Comparing the inverse Abel transform of this equation with the definition of the column density in Eq.(21), we obtain Eq.(27).
- [34] R.N. Bracewell, *The Fourier Transform and its Applications*, 3rd ed. (McGraw-Hill, 1999).

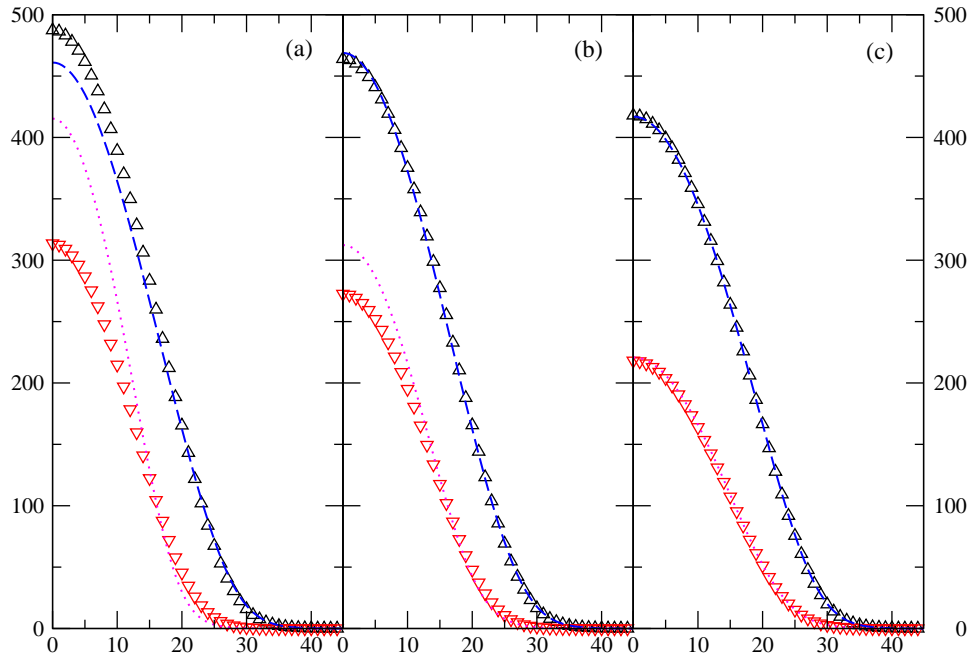


FIG. 1: (Color online) Comparison between density profiles of NSR fluctuation theory and that of Hartree-Fock approximation at weak coupling regime. Labels of horizontal and vertical axes are respectively dimensionless  $r/\ell$  and  $n(r)\ell^3$ . Up-spin and down-spin profiles calculated from fluctuation theory are represented by up-triangle and down-triangle, respectively. The dashed and dotted lines show the Hartree-Fock approximation to the up-spin and down-spin fermion profiles, respectively. The parameter range is chosen as  $N_\uparrow = 1.5 \times 10^7$ ,  $N_\downarrow = 5 \times 10^6$ , and  $T/T_F = 0.2$ . The interaction parameters  $-1/k_F a$  are respectively (a) 0.5 (b) 1.0 (c) 10.0

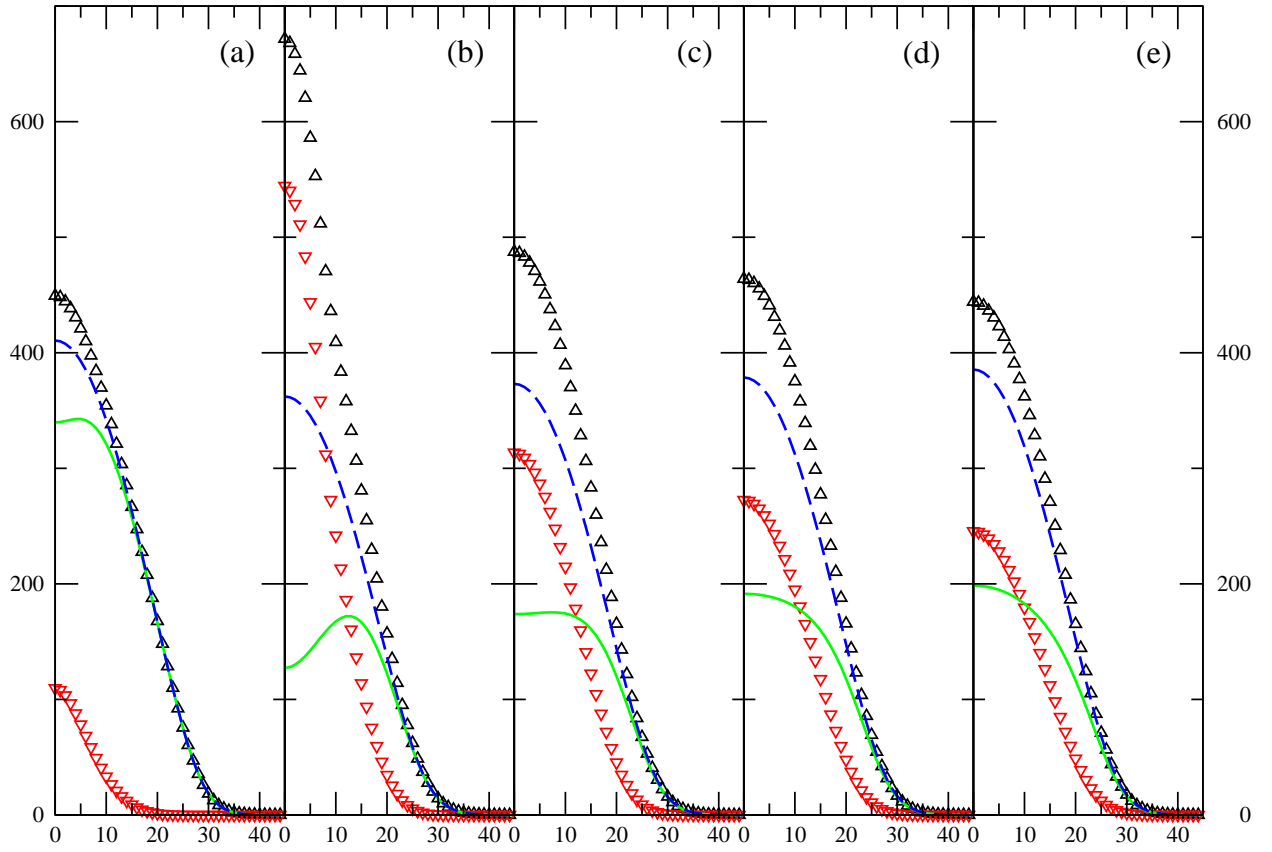


FIG. 2: (Color online) Density profiles of fermions of spin up and down. Labels of horizontal and vertical axes are respectively dimensionless  $r/\ell$  and  $n(r)\ell^3$ . Up-spin, down-spin, and excess fermion are represented by up-triangle, down-triangle, and solid line, respectively. The dashed lines shows the trapped non-interacting fermion fit to the wing of up-spin fermion profile. The dimensionless trap length  $k_F\ell = 28$ , and the temperature  $T/T_F = 0.2$ . The total populations of up-spin fermions  $N_\uparrow = 1.5 \times 10^7$ . In strong coupling regime (a), the interaction parameters  $-1/k_F a = -2.0$ , the total population of down-spin fermions  $N_\downarrow = 5 \times 10^5$  with the population imbalance  $\delta = 93\%$ . In weak coupling regime,  $-1/k_F a$  are respectively (b) 0.1 (c) 0.5 (d) 1.0 (e) 2.0,  $N_\downarrow = 5 \times 10^6$  with  $\delta = 50\%$ .

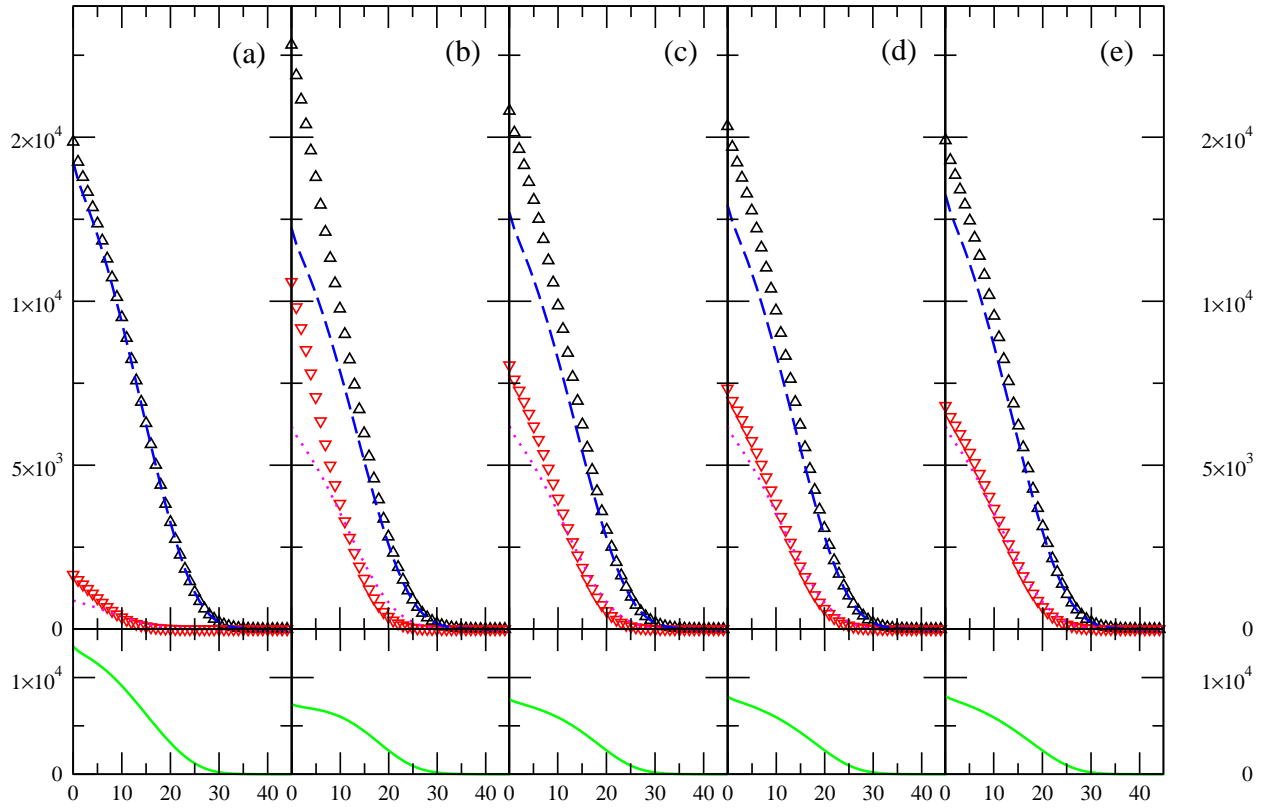


FIG. 3: (Color online) Column density profiles of fermions of spin up and down. Labels of horizontal and vertical axes are respectively dimensionless  $\rho/\ell$  and  $n_{\text{col}}(\rho)\ell^2$ . Up-spin, down-spin, and excess fermion are represented by up-triangle, down-triangle, and solid line (lower panels) respectively. The dashed line shows the trapped non-interacting fermion fit to the wing of spin-up fermion profile. The dotted line is the non-interacting down-spin fermion profile at the same temperature, total fermion numbers and trap length. Parameters are the same as in Fig 2.



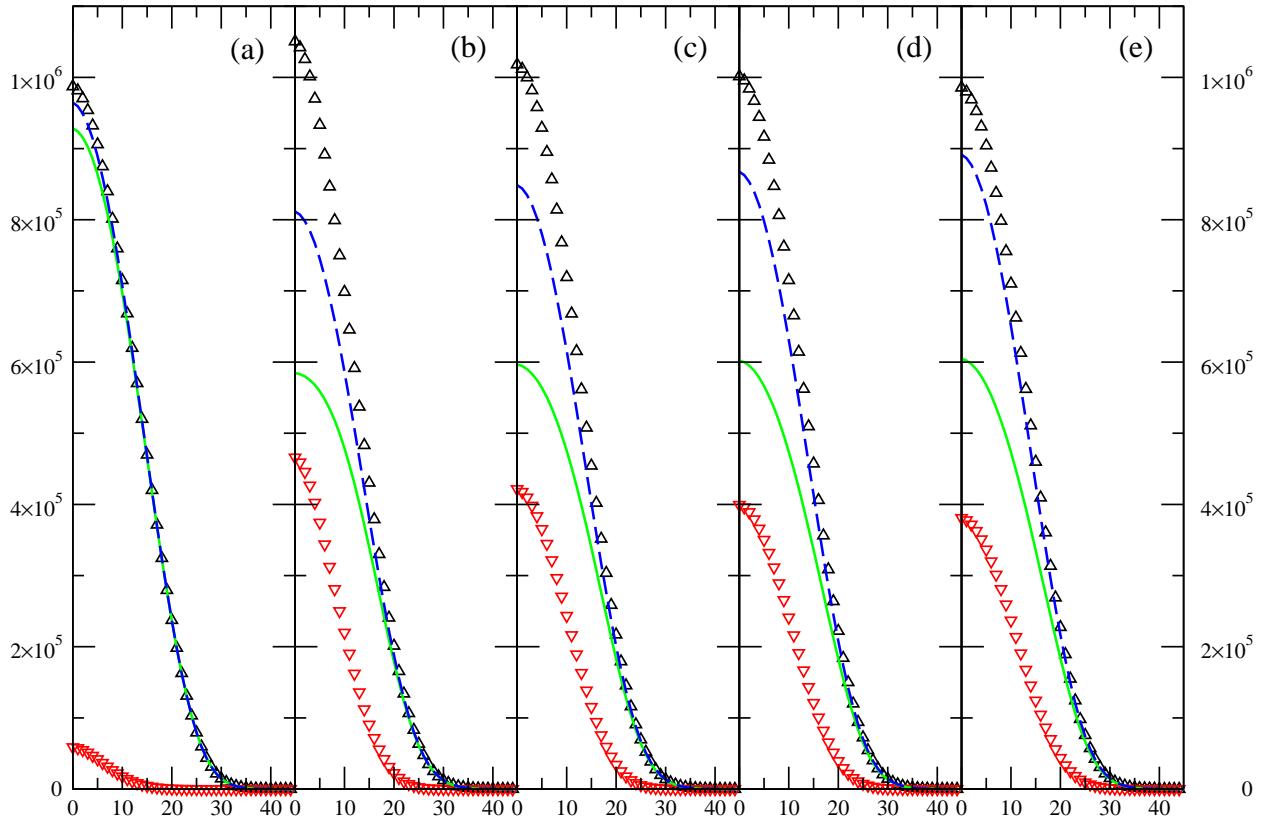


FIG. 4: (Color online) Axial density profiles of fermions of spin up and down. Labels of horizontal and vertical axes are respectively dimensionless  $z/l$  and  $n_{\text{axi}}(z)l$ . Up-spin, down-spin, and excess fermion are represented by up-triangle, down-triangle, and solid line, respectively. The dashed line shows the trapped non-interacting fermion fit to the wing of spin-up fermion profile. Parameters are the same as in Figs 2 and 3.